Bull. Chem. Soc. Ethiop. **2023**, 37(2), 515-532.
DOI: https://dx.doi.org/10.4314/bcse.v37i2.19

ISSN 1011-3924
Printed in Ethiopia
Online ISSN 1726-801X

PREPARATION, SPECTROSCOPIC, CYCLIC VOLTAMMETRY AND DFT/TD-DFT STUDIES ON FLUORESCEIN CHARGE TRANSFER COMPLEX FOR PHOTONIC APPLICATIONS

Ali A. Alkathiri[1], A.A. Atta[1*], Moamen S. Refat[2*], Tariq A. Altalhi[2], Sonam Shakya[3] Mohammed Alsawat[2], Abdel Majid A. Adam[2], Gaber A.M. Mersal[2] and A.M. Hassanien[4]

[1]Department of Physics, College of Science, Taif University, P.O. Box 11099, Taif 21944, Saudi Arabia
[2]Department of Chemistry, College of Science, Taif University, P.O. Box 11099, Taif 21944, Saudi Arabia
[3]Department of Chemistry, Aligarh Muslim University, Aligarh, 202002, India
[4]Department of Physics, College of Science and Humanities, Shaqra University, Al Quwaiiyah, Saudi Arabia

(Received August 22, 2022; Revised November 30, 2022; Accepted November 30, 2022)

ABSTRACT. The solid charge transfer (CT) complexes of fluorescein (Flu) with definite acceptors (tetrafluoro para benzoquinone (Fla); 7,7,8,8-tetracyanoquinodimethane (TCNQ); 2,3-dichloro-5,6-dicyano-p-benzoquinone (DDQ) and iodine) were prepared. Several characteristic analytic procedures such as transmission (FT-IR), diffuse reflectance, UV-Vis absorption, and cyclic voltammetry were used to determine the structural and optical properties of the prepared fluorescein charge transfer complex. Kubelka Munk model (K-M) and the absorption spectral fitting (ASF) methods were used to obtain the optical transitions of the solid fluorescein charge transfer complex and fluorescein CT complexes in methanol solution. The cyclic voltammetry method has been presented as capable of obtaining valuable information on quasi-reversible redox systems in the fluorescein CT-complexes. The electrochemical gap of the fluorescein CT complex was successfully determined from the cyclic voltammetry technique. Theoretical calculations (density functional theory) were made to corroborate experimental results for the synthesized CT complexes.

KEY WORDS: Fluorescein charge transfer complex, Optical spectroscopy, Cyclic voltammetry

INTRODUCTION

Modern organic electronic devices based on π-conjugated small molecules have attracted great concentration over recent years. These π-conjugated organic compounds offer numerous advantages, such as easy processability, inexpensiveness, lighter weight, and versatile molecular design. They are broadly applied as active materials for photovoltaic cells, bioelectronic devices, light-emitting diodes (LEDs), and field-effect transistors [1]. Significant studies have been devoted to explaining the transport mechanisms in organic semiconductor materials, carrier trapping phenomena, and charge injection processes to increase stability and electrical performance [2]. The organic charge-transfer complexes have created an excessive deal of consideration due to their successful physicochemical characteristics. The need for high-mobility organic semiconductor materials for high-performance electronic devices is speedily growing. Charge-transfer complexes play a significant role in smart sensors, optoelectronic devices, and stored chemical energy. The novel optoelectronic devices based on organic semiconductor materials need a good understanding of the charge-transport mechanism in organic semiconductors [3-5]. Charge-transfer complexes have attracted the consideration of scientific researchers due to their impressive applications in material science, engineering, pharmacology, medicine, and optoelectronic devices. The interaction between an electron-accepting molecule

*Corresponding author. E-mail: msrefat@tu.edu.sa (Moamen S. Refat); a.atta@tu.edu.sa (A.A. Atta)

(A) with an electron-donating molecule (D) forms a typical charge-transfer complex ($D + A \rightleftarrows [D.A]\ complex \rightleftarrows [D^{+}\cdot A^{-}\cdot]\ complex$). The formation of the donor-acceptor complex provides the advantages of new color with a broad absorption in the UV-Vis-NIR region as well as a controllable optical band gap and energy levels [6-14]. Fluorescein organic donor molecule is a red powder in the solid state and belongs to the xanthene family. Under UV-blue excitation, it emits a strong yellow-green light in a liquid solution. It is used in a wider range of modern applications due to its excellent fluorescence quantum yield, biocompatibility, and high molar absorptivity [15-18]. Tetrafluoro para benzoquinone (Fla), 7,7,8,8-tetracyanoquinodimethane (TCNQ), 2,3-dichloro-5,6-dicyano-*p*-benzoquinone (DDQ), iodine are usually used as acceptors materials to form charge-transfer complexes. For possible applications in photonic and materials science area, the present work is devoted to preparing solid charge-transfer complexes of fluorescein with definite acceptors mentioned above, then their structural, optical, and cyclic voltammetry characteristics were explored. Density functional theory (DFT/TD-DFT) was adopted to obtain the optimized structure of the CT complexes - [(Flu)(Fla)], [(Flu)(TCNQ)], and [(Flu)(DDQ)] with B-3LYP/6-31G (basis set). Experimental data were also corroborated theoretically through DFT.

EXPERIMENTAL

The fluorescein dye (Flu) was received from Aldrich Company, and used without further purification. DDQ, TCNQ, and Fla were obtained from Merck Company, and with prior use, they were purified by re-crystallization from $CHCl_3$. The solid CT complexes were synthesized by mixing 1 mmol of the donor in a methanol mixture with 1 mmol of DDQ, TCNQ, and Fla (acceptors) in the same solvent. At room temperature, the mixture was stirred for ~ 1 h. After reducing the solvent volume by the evaporation of 80%, the solid precipitate is obtained. The separated fluorescein CT complexes were filtered off, washed many times with chloroform ($CHCl_3$), and then the obtained solid precipitate of the CT complexes was dried under a vacuum. The diffuse reflectance spectra of the fluorescein CT-complex were recorded on Ocean Spectrometer model USB4000-XR1-ES. A Cary series spectrophotometer (Agilent Technologies) was used to measure the absorbance spectra of the fluorescein CT-complex over the range of 200-800 nm. The cyclic voltammetry (CV) measurements were described in detail in our published work [19]. To obtain the theoretical data for the CT complexes [(Flu)(Fla)], [(Flu)(TCNQ)], and [(Flu)(DDQ)], Gaussian 09RevD.01 program [20] was used with Pople's basic set B3LYP/6-31G, and Gradient corrected correlation [21]. B3LYP/6-31G level of theory was applied to obtain the optimized structure of [(Flu)(Fla)], [(Flu)(TCNQ)], and [(Flu)(DDQ)] CT complexes. A molecular electrostatic potential (MEP) map was also obtained to predict the reacting sites of the donor and acceptor molecules. Simulated IR frequencies was obtained for [(Flu)(Fla)], [(Flu)(TCNQ)], and [(Flu)(DDQ)] CT complexes. Animated modes of vibrations was used to assign the bands with full accuracy [21]. The simulated vibrational wavenumbers are often greater than the experimental values, according to the findings. The scaling factor should be used to scale the calculated wavenumbers in order to make a suitable comparison. LUMO (lowest unoccupied molecular orbital), HOMO (highest occupied molecular orbital), and energy gap was also calculated for [(Flu)(Fla)], [(Flu)(TCNQ)], and [(Flu)(DDQ)] CT complexes. For visualization of obtained DFT results, ChemCraft 1.5 software [22] was used.

RESULTS AND DISCUSSION

The infrared frequencies of the synthesized fluorescein charge transfer complexes have a change in the band intensities and the frequency which are attributed to the electronic configuration changes and the symmetry of the CT complex. The IR vibration bands at 719, 795, 894, 1166, 1548, 1668, and 2239 cm^{-1} of the free DDQ organic molecule can be attributed to ν(C–Cl), δ(C–C), ν(C=C), ν(C=O), and ν(C≡N), respectively. The IR spectrum of the free Fla acceptor has

some characteristic bands at 992 cm^{-1} for the ν(C–F), 1322 cm^{-1} for the ν(C=C stretching), and (1745 and 1672) cm^{-1} for the ν(C=O stretching). The IR vibration bands at 719, 795, 894, 1166, 1548, 1668, and 2239 cm^{-1} of the free TCNQ organic molecule can be attributed to 850 cm^{-1}, (1043 and 1116), 1346,1531, (2091 and 2208), 2963, and 3044 cm^{-1} can be attributed to δ_r(C–H), δ(C–C), δ(C–H), ν(C=C), ν(C≡N), ν_s(C–H) and ν_{as}(C–H) vibration motions. From the IR vibration bands of the Flu organic donor molecule and the corresponding acceptors, it can be recognized that the ν(C≡N), ν(C-F), ν(C=O), and ν(C-Cl) vibration motions are shifted to higher or lower frequencies values in case of complexes.

The diffused reflectance spectroscopy (R_d) is a significant procedure to explore the qualitative knowledge about the optical properties of the investigated fluorescein CT-complex in powder form (inhomogeneous media). Figure 1 shows the diffuse reflectance spectra (R_d) of fluorescein CT-complex. The Kubelka-Munk model (K-M) is used to convert the diffuse reflectance spectra of the fluorescein CT-complex into absorption spectra [23-29].

$$R_d = \frac{R_{Sample}}{R_{BaSO_4}} \tag{1}$$

$$F(R_d) = \frac{(1 - R_d)^2}{2R_d} \tag{2}$$

$$F(R_d) \propto \alpha(h\nu) \propto \frac{(h\nu - E_g)^2}{h\vartheta} \tag{3}$$

where $F(R_d)$ is the Kubelka-Munk function and α is the absorption coefficient of the fluorescein CT-complex. Figure 1 (A-E) shows $(F(R_d)h\nu)^{1/2}$ versus ($h\nu$) for fluorescein CT-complexes. The estimated values of the allowed indirect gap are given in Table 1.

Table 1. Energy gap electronic transitions of the fluorescein charge transfer complex according to DRS, ASF and CV.

Sample	E_g^{DRS} (eV)		E_g^{ASF} (eV)				E_g^{CV} (eV)
Fluorescein dye	2.09	2.25	2.34	3.682	1.98	--	1.96
[(Flu)(I_2)] complex	2.14	-	2.482	2.678	3.571	2.36	1.96
[(Flu)(DDQ)] complex	2.21	2.1	2.455	3.075	3.534	2.24	2.48
[(Flu)(Fla)] complex	2.12	-	2.504	3.608	2.68	2.33	2.1
[(Flu)(TCNQ)] complex	2.19	-	2.507	4.029	--	--	2.53

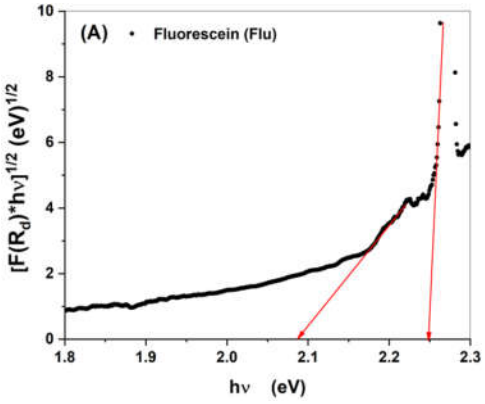

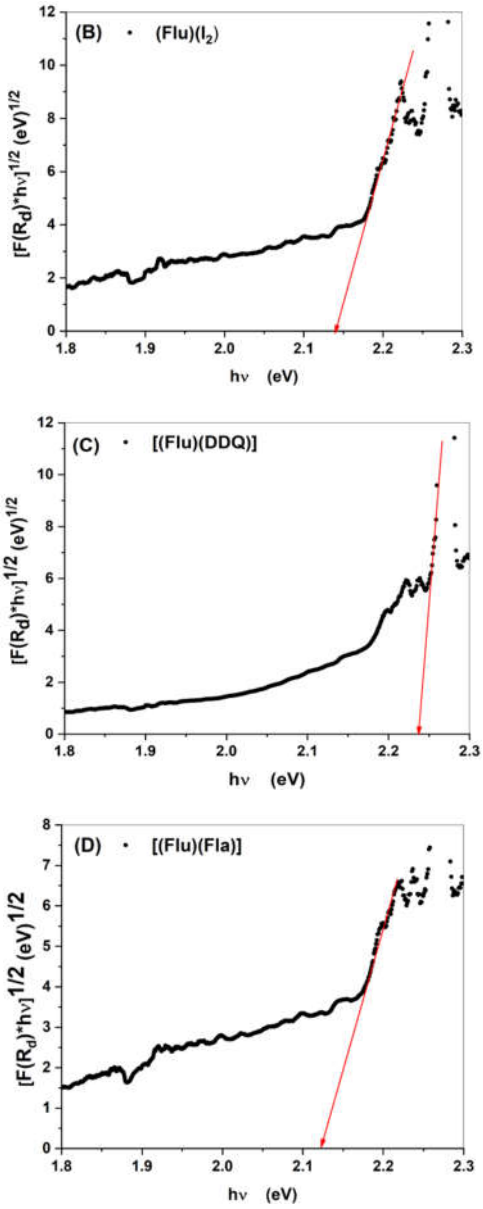
(B) • (Flu)(I2)
[F(Rd)*hν]1/2 (eV)1/2
hν (eV)
(C) • [(Flu)(DDQ)]
[F(Rd)*hν]1/2 (eV)1/2
hν (eV)
(D) • [(Flu)(Fla)]
[F(Rd)*hν]1/2 (eV)1/2
hν (eV)

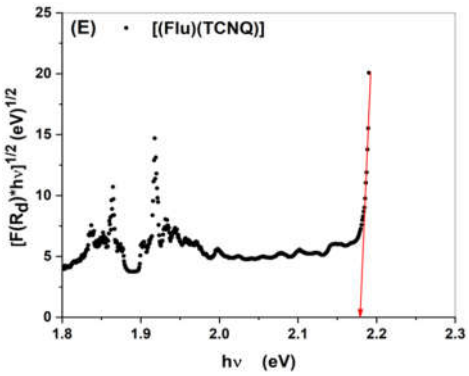

Figure 1. The diffuse reflectance spectra of solid fluorescein charge transfer complex, and (A-E): The Kubelka–Munk relation versus photon energy of the solid fluorescein charge transfer complex

UV-Vis spectroscopy is an important tool to identify the energy position, intensity, and individual electronic bands of fluorescein CT complexes in methanol solution. Figure 2 shows the electronic absorption spectra of fluorescein CT complexes in methanol. The molar absorptivity (ε_{molar}) of the fluorescein CT-complexes can be used to estimate the oscillator strengths (*f*) and the electric dipole strength (q^2) from the following relations [29-33]:

$$q^2 = \frac{1}{2500}\varepsilon_{molar}\left(\frac{\Delta\bar{\upsilon}}{\bar{\upsilon}}\right), \tag{4}$$

$$f = 4.3 \times 10^{-9} \int \varepsilon_{molar}\, d\bar{\upsilon}, \tag{5}$$

where $\bar{\upsilon}$ is the wavenumber and $\Delta\bar{\upsilon}$ is the absorption half-band width. The spectral behavior of the molar absorptivity for the fluorescein CT complexes is displayed in Figure 2(A-E). A Gaussian fitting with asymmetric least squares smoothing baseline was done to calculate *f* and q^2. The Gaussian fitting analysis and the calculated values of (q^2) and (*f*) for fluorescein CT-complex in methanol (C = 5×10^{-7} M/L) are shown in Table 2.

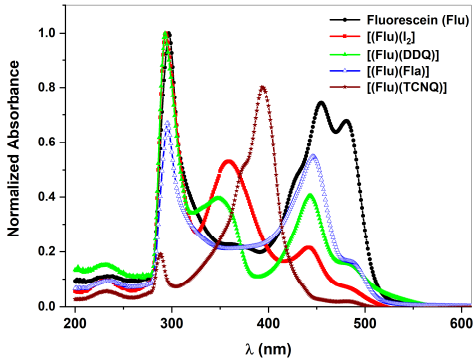

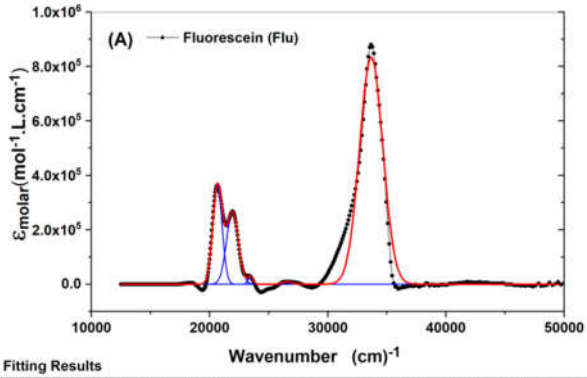

Fitting Results

Peak Index	Peak Type	Area Intg	FWHM	Max Height	Center Grvty	Area IntgP
1	Gaussian	3.60162E8	936.43811	361315.81724	20661.15702	13.04224
2	Gaussian	3.31058E8	1177.34894	264159.63256	21929.82456	11.9883
3	Gaussian	2.04597E9	2305.75235	833595.57659	33670.03367	74.08907
4	Gaussian	1.41819E7	481.36307	27677.62878	23476.77596	0.51356
5	Gaussian	1.01302E7	892.95898	10657.44	26576.1612	0.36683

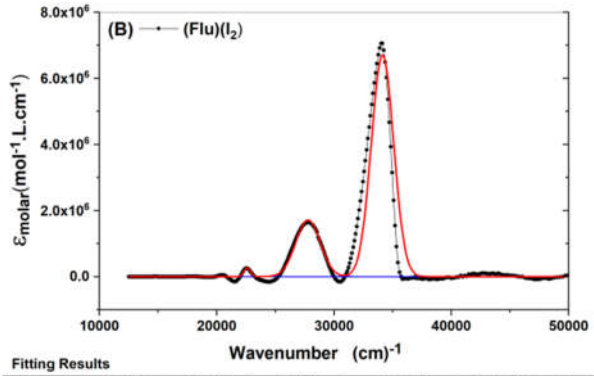

Fitting Results

Peak Index	Peak Type	Area Intg	FWHM	Max Height	Center Grvty	Area IntgP
1	Gaussian	4.48246E9	2453.28168	1.71647E6	27777.77778	21.76381
2	Gaussian	1.5929E10	2228.98683	6.71351E6	34129.69283	77.34063
3	Gaussian	1.84449E8	645.29521	268525.54531	22588.79781	0.89556

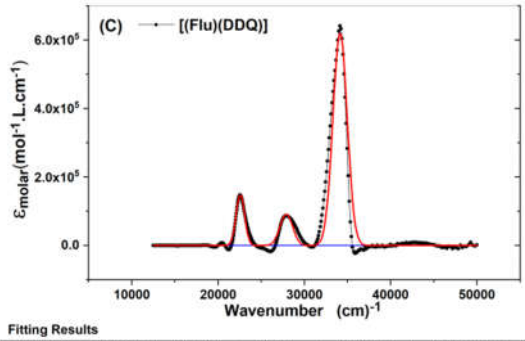

Fitting Results

Peak Index	Peak Type	Area Intg	FWHM	Max Height	Center Grvty	Area IntgP
1	Gaussian	1.84188E8	1171.22378	147736.847	22573.36343	11.26185
2	Gaussian	1.28182E9	1940.38762	620592.8201	34129.69283	78.37479
3	Gaussian	1.69493E8	1736.25487	91707.66189	27899.59016	10.36335

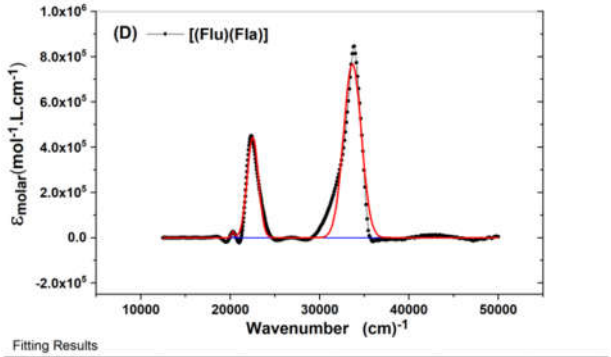

Fitting Results

Peak Index	Peak Type	Area Intg	FWHM	Max Height	Center Grvty	Area IntgP
1	Gaussian	6.93653E8	1467.97111	443907.67373	22514.6656	26.59725
2	Gaussian	1.90302E9	2327.99561	767943.16467	33673.68623	72.96892
3	Gaussian	1.13142E7	383.02331	27750.2847	20304.58327	0.43383

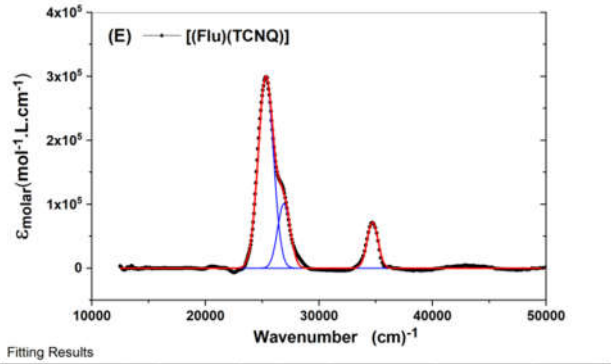

Fitting Results

Peak Index	Peak Type	Area Intg	FWHM	Max Height	Center Grvty	Area IntgP
1	Gaussian	4.99119E8	1564.74485	299659.61323	25316.4557	68.72334
2	Gaussian	8.67363E7	1127.47698	72270.48091	34722.22222	11.94266
3	Gaussian	1.40418E8	1308.05973	100846.70258	26909.15301	19.334

Figure 2. Spectral behavior of the normalized absorbance of the fluorescein charge transfer complex in methanol, and (A-E): The Gaussian fitting analysis of molar absorptivity for the fluorescein charge transfer complex in methanol.

Table 2. The oscillator strengths (*f*) and the electric dipole strength (q^2) of the fluorescein charge transfer complex in methanol.

Sample	Oscillator strengths (*f*)					Electric dipole strength (q^2)				
Fluorescein dye	1.55	1.42	10.03	0.61	0.04	6.55	5.67	22.83	0.23	0.14
[(Flu)(I_2)] complex	19.28	68.50	0.79	-	-	60.64	175.4	3.11	-	-
[(Flu)(DDQ)] complex	0.79	5.51	0.73	-	-	3.07	14.11	22.84	-	-
[(Flu)(Fla)] complex	2.98	8.18	0.486	-	-	1.16	21.24	0.21	-	-
[(Flu)(TCNQ)] complex	2.15	0.42	0.60	-	-	7.41	0.94	1.96	-	-

The absorption spectrum fitting (ASF) method can be applied to precisely determine the optical band gap energies of fluorescein CT-complex in the UV-Vis region [34-42]:

$$E_g(eV) = \frac{hc}{\lambda_{gap}} = \frac{1239.83}{\lambda_{gap}} \tag{6}$$

$$A\,(\lambda) = \frac{d}{2.303}\, Z(hc)^{n-1}\lambda\left(\frac{1}{\lambda} - \frac{1}{\lambda_{gap}}\right)^n \tag{7}$$

$$ln\left(\frac{A}{\lambda}\right) = \ln(D) + n\, ln\left(\frac{1}{\lambda} - \frac{1}{\lambda_{gap}}\right) \tag{8}$$

where n is the power taking the value of 2 for the allowed indirect transition, A is optical absorbance, Z is a constant, c is the velocity of light, and d is the thickness of the sample (1 cm).

Figure 3 (A-E) shows a relation between $\left(\frac{A}{\lambda}\right)^{1/2}$ against $(1/\lambda)$ for fluorescein CT-complexes. From this figure, the optical band gap (E_{gap}^{ASF}) can be estimated and listed in Table 2.

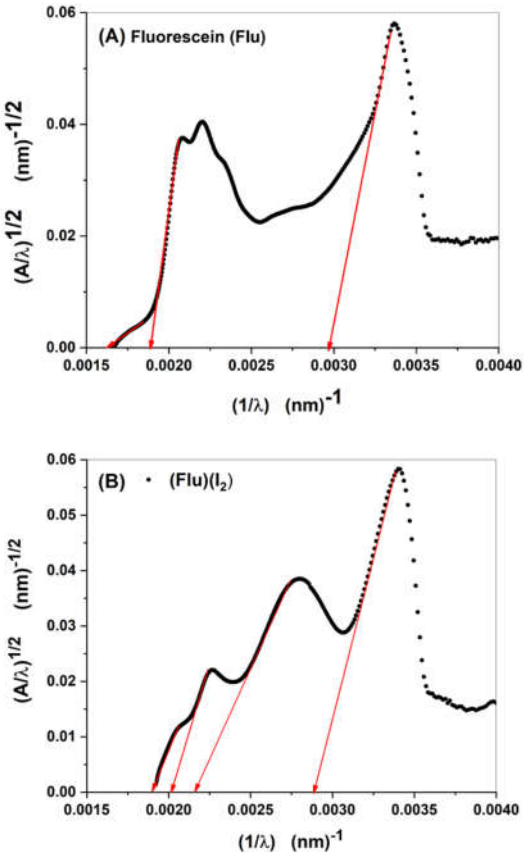

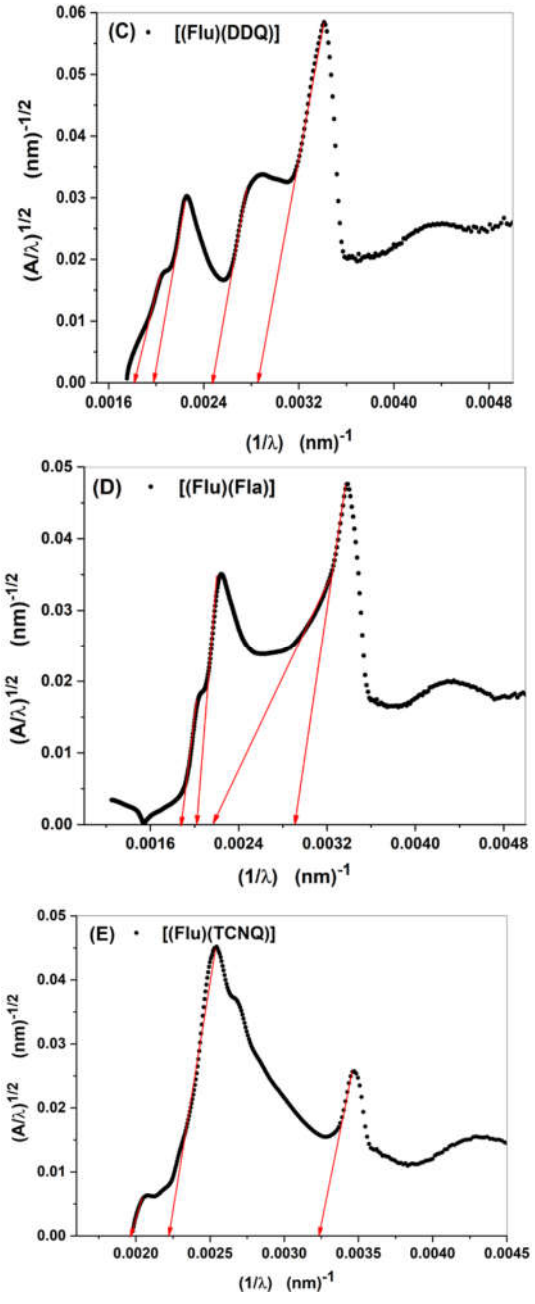

Figure 3 (A-E). The relation between $\left(\frac{A}{\lambda}\right)^{1/2}$ against $(1/\lambda)$ for the fluorescein charge transfer complex in mehanol.

Figure 4-A depicts the cyclic voltammogram for fluorescein dye, which revealed two quasi-reversible redox systems [43]. The first system's oxidation peak (E_{pa1}) was found to be +0.13 V, while the cathodic peak (E_{pc1}) was observed to be -0.06 V. The reversibility of the reaction was demonstrated by the difference between the anodic and cathodic peak potentials (ΔE), which was determined to be equal to + 0.19 V. The formal potential ($E_{1/2}$) was taken as the average of E_{pc1} and E_{pa1} is +0.035 V. In the second system, E_{pa2} and E_{pc2} appeared at+0.62 V and +0.55 V respectively. The calculated ΔE was found + 0.07 V and $E_{1/2}$ is + 0.62 V [43-45].

$$E_{HOMO} = -(E_{onset\,(oxidation)} + 4.4)\ eV \quad (9)$$

$$E_{LUMO} = -(E_{onset\,(reduction} + 4.4)\ eV \quad (10)$$

$E_{(onset\ oxidation)}$ and $E_{(onset\ reduction)}$ peak values have been calculated to be 1.28 V and 0.68 V, respectively. HOMO, LUMO, and band gap ($\boldsymbol{E_g^{CV}}$) were calculated to be, -5.68, -3.72, and 1.96 eV, respectively.

The electrochemical behavior of the [(Flu)(I_2)] complex under the previously specified circumstances is shown in Figure 4-B using cyclic voltammetry. Two quasi-reversible redox systems and one irreversible cathodic peak were depicted in this figure. In the first redox system, E_{pc1} occurred at +0.07 V, whereas E_{pa1} occurred at +0.37 V. ΔE was found to be +0.3 V, with +0.22 V $E_{1/2}$. The E_{pa2} came at + 0.65 V in the second redox system, whereas E_{pc2} appeared at +0.43 V. ΔE and $E_{1/2}$ were determined to be + 0.22 V and + 0.54 V, respectively.

The irreversible cathodic peak appeared at -0.37 V. The [(Flu)(I_2)] complex also showed an irreversible cathodic peak at -0.47 V and an anodic peak at +0.9 V. $E_{(onset\ oxidation)}$ and $E_{(onset\ reduction)}$ peak values were determined to be +1.3 V and -0.66 V, respectively. The computed HOMO, LUMO, and band gap ($\boldsymbol{E_g^{CV}}$) were -5.7 eV, -3.77 eV, and 1.96 eV, respectively.

The electrochemical behavior of the [(Flu)(DDQ)] complex is depicted in Figure 4-C using the cyclic voltammetric method. Two quasi-reversible redox systems and two irreversible cathodic peaks were seen in the [(Flu)(DDQ)] complex. At -1.14 V, an irreversible cathodic peak developed, whereas an anodic peak appeared at +0.2. For the two quasi-reversible redox couples, E_{pa1} appeared at -0.32 V whereas E_{pc1} appeared at -0.42 V. The values for ΔE and $E_{1/2}$ are +0.1 V and -0.37 V, respectively. The E_{pa2} emerged at +0.73 V in the second system, whereas the E_{pc2} arrived at +0.53 V. ΔE was determined to be +0.2 V, while $E_{1/2}$ was found to be +0.625 V. The $E_{(onset\ oxidation)}$ and $E_{(onset\ reduction)}$ peaks are +1.3 V and -1.18 V, respectively. The calculated values for HOMO, LUMO, and the band gap ($\boldsymbol{E_g^{CV}}$) are -5.7, -3.22, and 2.48 eV, respectively.

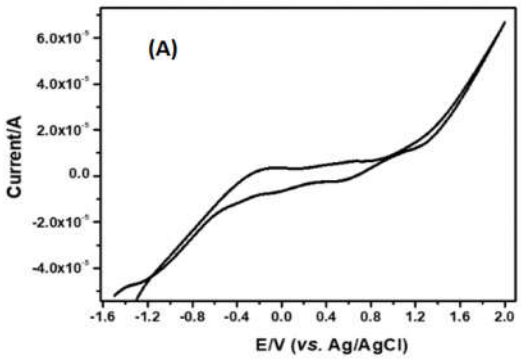

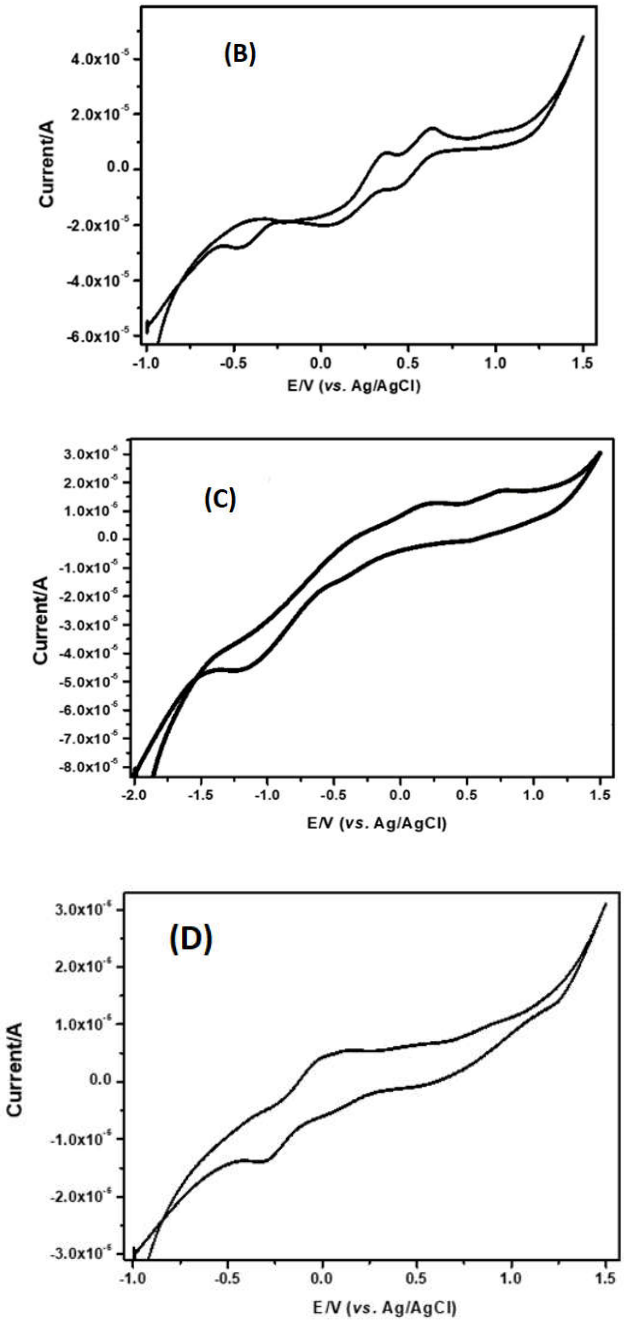
(B)
Current/A
E/V (vs. Ag/AgCl)
(C)
Current/A
E/V (vs. Ag/AgCl)
(D)
Current/A
E/V (vs. Ag/AgCl)

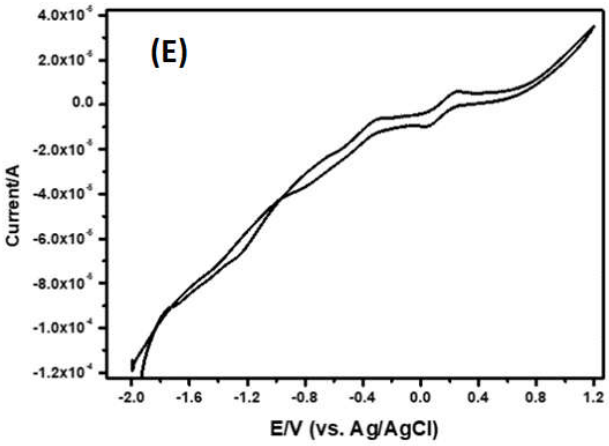

Figure 4. Cyclic voltamnmetry of the (A): fluorescein dye, (B): [(Flu)(I_2)] complex, (C): ([(Flu)(DDQ)] complex, (D): [(Flu)(Fla)] complex and (E): [(Flu)(TCNQ)] complex using Pt wire as a working electrode in dichloromethane in the presence of 0.1 M tetrabutlammonium perchlorate and 100 mV/s scan rate.

Figure 4-D depicts the cyclic voltammetry [(Flu)(Fla)] complex using a Pt electrode in DCM in the presence of TBAP. The [(Flu)(Fla)] complex has one anodic peak at -0.34 V and three quasi-reversible redox systems. The first quasi-reversible redox pairs E_{pa1} and E_{pc1} were seen at 0.0 V and -0.31 V, respectively. Calculated values for ΔE and $E_{1/2}$ are +0.31 V and -0.155 V, respectively. In the second oxidation-reduction system, E_{pc2} showed up at +0.06 V while E_{pa2} showed up at +0.47 V. The ΔE was calculated and found +0.41 V, while the $E_{1/2}$ was 0.265 V. The third quasi-reversible redox couple, E_{pa3}, appeared at +0.92V, while E_{pc3} appeared at +0.57 V. The ΔE was found to be -0.35 V, with $E_{1/2}$ obtaining at +0.745 V. The obtained values for the E(onset oxidation) and E(onset reduction) peaks are +1.35 and -0.75 V, respectively, while the calculated HOMO, LUMO, and band gap ($\boldsymbol{E_g^{CV}}$) were -5.75, -3.65, and 2.1 eV, respectively. The electrochemical behavior of the [(Flu)(TCNQ)] complex under the previously specified circumstances is shown in Figure 4-E using cyclic voltammetry. Two irreversible peaks, one cathodic peak at -1.2 V and one anodic peak at -0.3 V, as well as two quasi-reversible redox systems, could be seen in this graph. E_{pa1} was detected at -0.63 V, while E_{pc1} was detected at -0.81 V. The calculated E was determined to be +0.18 V, with a formal potential of -0.72 V. E_{pa1} and E_{pc1} were found to be -0.63 V and -0.81 V, respectively. The computed ΔE was +0.18 V, with a formal potential of -0.72 V. In the second redox system, E_{pa2} occurred at + 0.25 V while E_{pc2} appeared at + 0.4 V. ΔE and $E_{1/2}$ were calculated to be + 0.21 and + 0.145 V, respectively. The peaks for $E_{(onset\ oxidation)}$ and $E_{(onset\ reduction)}$ are, respectively, -0.83 and -1.7 V. The band gap ($\boldsymbol{E_g^{CV}}$), HOMO, and LUMO calculated values were 5.23, -2.7, and 2.53 eV, respectively.

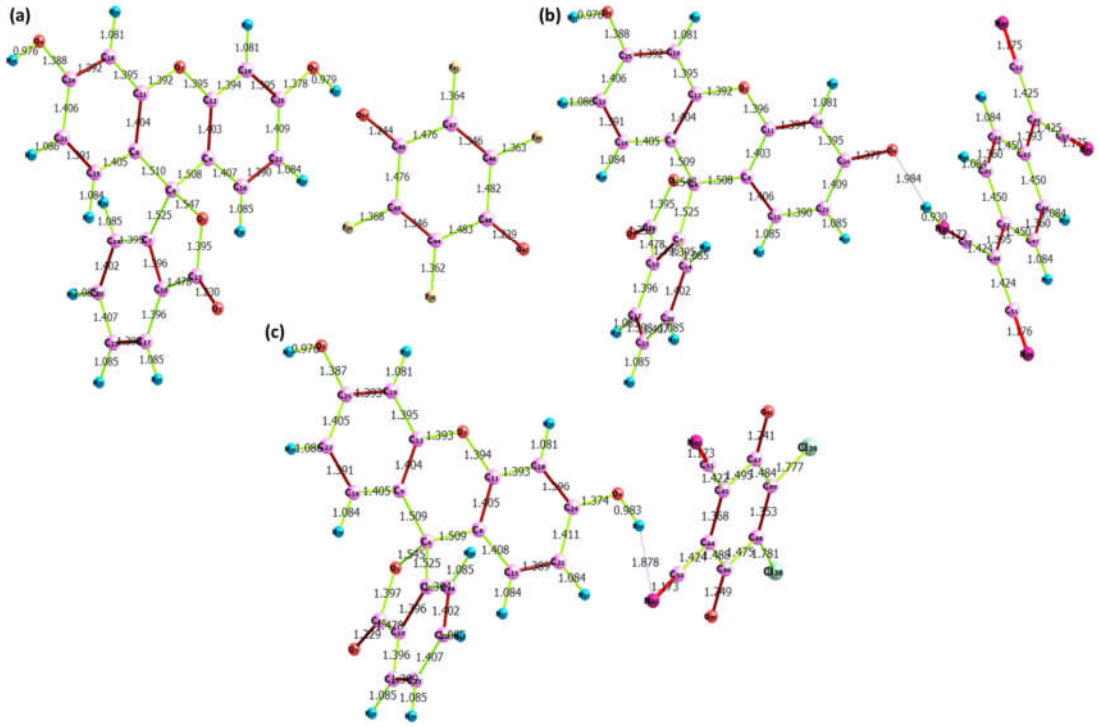

Figure 5. Optimized structure of (a) [(Flu)(Fla)], (b) [(Flu)(TCNQ)], and (c) [(Flu)(DDQ)] complex (B3LYP/ 6-31G) showing bond lengths.

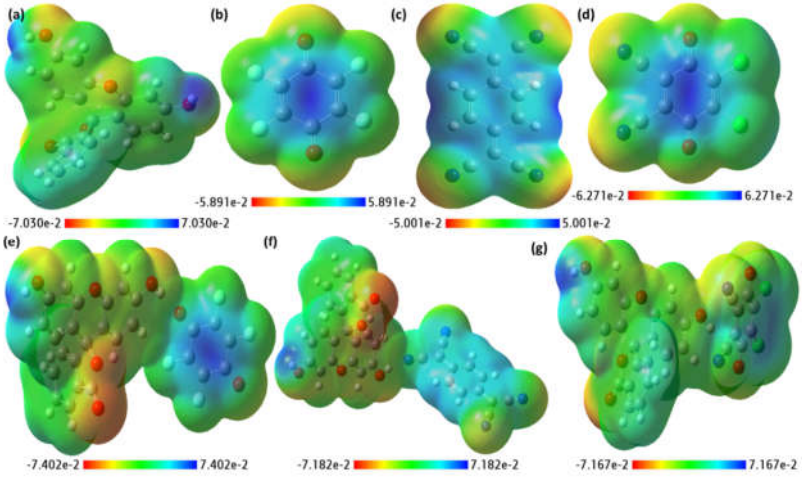

Figure 6. MEP surface map of (a) Flu, (b) Fla, (c) TCNQ, (d) DDQ, (e) [(Flu)(Fla)], (f) [(Flu)(TCNQ)], and (g) [(Flu)(DDQ)] (B3LYP/ 6-31G) with respective color scales.

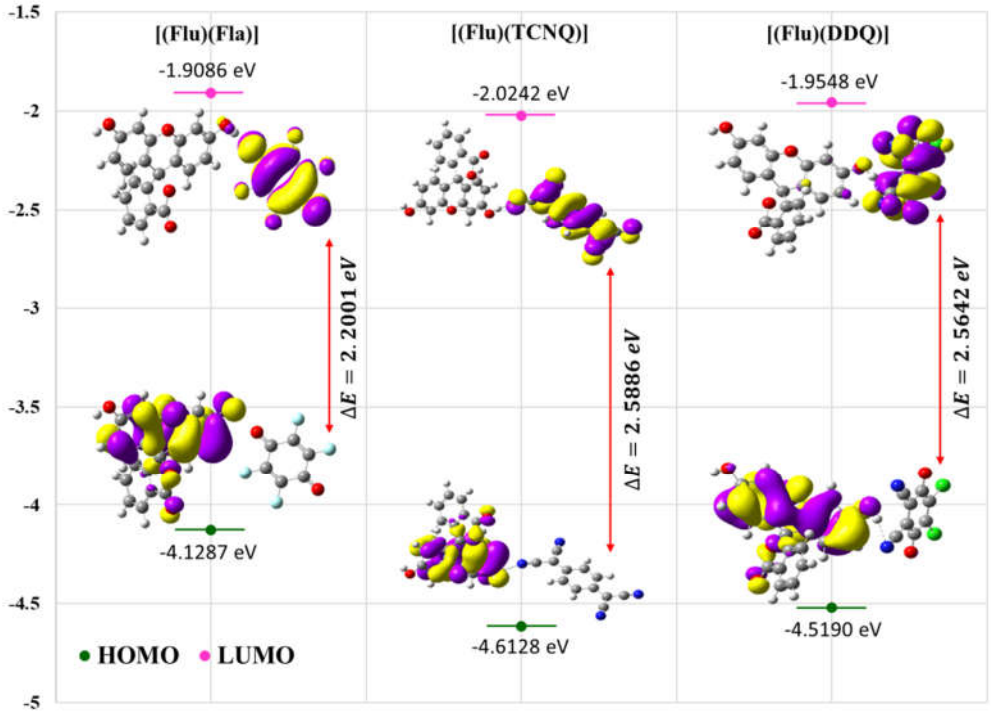

Figure 7. The spatial plot of HOMO and LUMO with their energy gap for [(Flu)(Fla)], [(Flu)(TCNQ)], and [(Flu)(DDQ)] complex.

The structure of [(Flu)(Fla)], [(Flu)(TCNQ)], and [(Flu)(DDQ)] was optimized through B3LYP/6-31G, and the geometry is represented in Figure 5 with Mulliken atomic numbering scheme. Figure 6 represents the optimized structures of [(Flu)(Fla)], [(Flu)(TCNQ)], and [(Flu)(DDQ)] showing all the bond lengths in Å. The molecular electrostatic potentials strength of reactants (Flu, Fla, TCNQ, and DDQ) and CT complex {[(Flu)(Fla)], [(Flu)(TCNQ)], and [(Flu)(DDQ)]} is presented through MEP map (molecular electrostatic potential), as shown in Figure 6. The electropositive region lies around OH and CH atoms of Flu, shown with the blue area and the electronegative region lies around N and O atoms of acceptor moieties, shown with the red area. This gives us the idea regarding preferential binding sites for the electrophilic and nucleophilic attacks. The MEP surface of reactants (Flu, Fla, TCNQ, and DDQ) and CT complex {[(Flu)(Fla)], [(Flu)(TCNQ)], and [(Flu)(DDQ)]} is plotted from deep red to deep blue color scale (Figure 6) [46].

In the gas phase, the TD-DFT approach was employed to investigate the nature of the electronic transitions in [(Flu)(Fla)], [(Flu)(TCNQ)], and [(Flu)(DDQ)]. For [(Flu)(Fla)], [(Flu)(TCNQ)], and [(Flu)(DDQ)] electronic absorption band is obtained at 558, 478, and 483 nm, respectively. The HOMO (-4.1287 eV) to LUMO (-1.9086 eV) energy gap (ΔE) was calculated to be 2.2001 eV for [(Flu)(Fla)] complex. For [(Flu)(TCNQ)] complex HOMO (-4.6128 eV) to LUMO (-2.0242), ΔE = 2.5886, and for [(Flu)(DDQ)] complex HOMO (-4.5190 eV) to LUMO (-1.9548), ΔE = 2.5642. The LUMOs are present in the acceptor moieties of the CT complexes, while HOMOs can be seen in the donor moiety of the CT complexes. The FMO

with energy gap for the CT complexes are represented in Figure 7 [47-50]. Some important molecular parameters of [(Flu)(Fla)], [(Flu)(TCNQ)], and [(Flu)(DDQ)] obtained in the gas phase based on HOMO-LUMO and optimized structure are provided in Table 3.

Table 3. Various other theoretical molecular parameters of CT complexes.

Parameters	B3LYP/ 6-31G		
	[(Flu)(Fla)]	[(Flu)(TCNQ)]	[(Flu)(DDQ)]
Minimum SCF energy (a.u.)	-1923.316617	-1823.555850	-2630.044148
Polarizability (α) (a.u.)	401.394611	431.731227	653.600049
Dipole moment (Debye)	5.809081	5.000880	5.347966
Zero point vibrational energy (kcal/mol)	206.31742	254.29036	212.53203
Total thermal energy (kcal/mol)	225.390	275.749	233.146
Electronic spatial extent (a.u.)	21242.3411	37685.4500	37469.6323
Frontier MO energies (eV)			
LUMO	-1.9086	-2.0242	-1.9548
HOMO	-4.1287	-4.6128	-4.5190
Gap (HOMO – LUMO)	2.2201	2.5886	2.5642

CONCLUSION

The solid CT complexes of fluorescein dye with definite acceptors [DDQ, TCNQ, Fla, and I_2] mentioned above were prepared. Infrared frequencies and tentative assignments for the fluorescein charge transfer complex were studied. The indirect allowed optical band gaps of the solid fluorescein charge transfer complex were determined by using the Kubelka-Munk model. The indirect allowed optical band gaps of the fluorescein charge transfer complex in methanol were estimated by using absorption spectral fitting (ASF).The molar absorptivity of the fluorescein CT complexes were used to estimate the oscillator strengths and the electric dipole strength. The cyclic voltammetry technique is used to calculate the HOMO, LUMO, and the electrochemical gap of the fluorescein CT complexes. A comparison of the optical and electrochemical band gaps shows that the differences do not exceed ±0.20 eV. DFT calculations provided the optimized geometry of [(Flu)(Fla)], [(Flu)(TCNQ)], and [(Flu)(DDQ)] CT complex with minimum energy. Experimental data were also corroborated theoretical through DFT and found then in good agreement. The obtained data are vital for applied material science research fields such as organic photonic applications.

ACKNOWLEDGEMENT

Taif University Researchers Supporting Project number (TURSP-2020/22), Taif University, Taif, Saudi Arabia.

REFERENCES

1. Dai, X.; Meng, Q.; Zhang, F.; Zou, Y.; Di, C.; Zhu, D. Electronic structure engineering in organic thermoelectric materials. *J. Energy Chem.* **2021**, 62, 204-219.
2. Liguori, R.; Rubino, A. Admittance spectroscopy and material modeling for organic electronicapplications. *Mater. Today: Proc.* **2021**, 44, 2033-2037.
3. Wang, Y.; Qin, W. Light-driven molecular motion modifying the electronic structure and spin properties of solid organic superstructure. *Org. Electron.* **2021**, 92, 106103.
4. Li, Y.; Yi, Y.; Cui, B.; Chen, J. Two-dimensional electronic and charge-transport properties of a monolayerorganic crystal: Impacts of the collinear transfer-integral correlations. *Org. Electron.* **2020**, 78, 105609.

5. Alrooqi, A.; Al-Amshany, Z.M.; Al-Harbi, L.M.; Altalhi, T.A.; Refat, M.S.; Hassanien, A.M.; Atta, A.A. Impact of charge transfer complex on the dielectric relaxation processes in poly(methyl methacrylate) polymer. *Molecules* **2022**, 27, 1993.
6. Adam, A.A.; Refat, M.S.; Altalhi, T.A.; Aldawsari, F.S. Charge-transfer (CT) dynamics of triamterene with 2,3-dichloro-5,6-dicyano-p-benzoquinone acceptor: A n→π* model CT complex generated by liquid- and solid-state reactions. *J. Mol. Liq.* **2021**, 334, 116119.
7. Balraj, C.; Balaji, S.; Karthikeyan, M. Systematic measurements of charge transfer complexes caused from 1-phenyl-1,2,3,4-tetrahydroisoquinoline and 4-aminoacetanilide with series of π-acceptors (BQ, DDQ, TCNQ). *Spectrochim. Acta A Mol. Biomol. Spectrosc.* **2021**, 245, 118931.
8. Adam, A.A.; Altalhi, T.A.; Saad, H.A.; Alsuhaibani, A.M.; Refat, M.S.; Hegab, M.S. Correlations between spectroscopic data for charge-transfer complexes of two artificial sweeteners, aspartame and neotame, generated with several π-acceptors. *J. Mol. Liq.* **2021**, 333, 115904.
9. Altalhi, T.; Gobouri, A.A.; Refat, M.S.; El-Nahass, M.M.; Hassanien, A.M.; Atta A.A.; Al Otaibi, S.; Kamal, A.M. Optical spectroscopic studies on poly(methyl methacrylate) doped by charge transfer complex. *Opt. Mater.* **2021**, 117, 111152
10. Adam, A.A.; Saad, H.A.; Alsuhaibani, A.M.; Refat, M.S.; Hegab, M.S. Charge-transfer chemistry of azithromycin, the antibiotic used worldwide to treat the coronavirus disease (COVID-19). Part III: A green protocol for facile synthesis of complexes with TCNQ, DDQ, and TFQ acceptors. *J. Mol. Liq.* **2021**, 335, 116250.
11. Adam, A.A.; Altalhi T.A.; Saad, H.A.; Refat, M.S.; Hegab, M.S. Exploring the charge-transfer chemistry of fluorine-containing pyrazolin-5-ones: The complexation of 1-methyl-3-trifluoromethyl-2-pyrazoline-5-one with five π-acceptors. *J. Mol. Liq.* **2021**, 331 115814.
12. Shen, J.; Wang, W.; Zhang, S.; Gao, J.; Xia, R.; Huang, X.; Jiang, S.; Wang, H. A fluorescein sodium wide-area pH optical sensor based on amplification characteristics. *Opt. Commun.* **2021**, 493, 127030.
13. Yamaguchi, I.; Matsumoto, Y.; Miyoshi, K.; Wang, A. Synthesis, properties and graft polymerization of ionic conjugated polymers with TCNQ anion radical. *Polymer* 2021, 219, 123552.
14. Zhong, Y.; Li, Y.; Meng, J.; Lin, X.; Huang, Z.; Shen, Y.; Huang, Y. Boosting the cyclability of tetracyanoquinodimethane (TCNQ) as cathode material in aqueous battery with high valent cation. *Energy Storage Mater.* **2021**, 43, 492-498.
15. Legentil, P.; Leroux, F.; Therias, S.; Mahiou, R.; Chadeyron, G. Revisiting fluorescein and layered double hydroxide using a synergistic approach: A complete optical study. *J. Lumin.* **2019**, 215, 116634.
16. Jin, J.-Y.; Kim, H.-G.; Hong, C.-H.; Suh, E.-K.; Lee, Y.-S. White light emission from a blue LED, combined with a sodium salt of fluorescein dye. *Synth. Met.* **2007**, 157, 138-141.
17. Nganga, J.B.; Jung, Y.J.; Si, Y.; Kim, M.; Ko, H.; Hwang, G.T.; Lee, H.J.; Lee, H.-I.; Lee, J. K. Photoinduced radical polymerization by methyl fluoresceins under visible light and the application to signal amplification of hydrogen peroxide. *Dyes Pigm.* **2022**, 200, 110163.
18. Iqbal, J.; Yahia, I.S.; Zahran, H.Y.; AlFaify, S.; AlBassam, A.M.; El-Naggar, A.M. Linear and non-linear optics of nano-scale 2′, 7′ dichloro-fluorescein/FTO optical system: Bandgap and dielectric analysis. *Opt. Mater.* **2016**, 62, 527-533.
19. Alrooqi, A.; Al-Amshany, Z.M.; Al-Harbi, L.M.; Altalhi, T.A.; Refat, M.S.; Hassanien, A.M.; Mersal, G.A.M.; Atta, A.A. Spectroscopic and physicochemical studies on 1,2,4-triazine derivative. *Coatings* **2022**, 12, 714.
20. Becke, A.D. Density-functional thermochemistry. III. The role of exact exchange. *J. Chem. Phys.* **1993**, 98, 5648-5652.
21. Hariharan, P.C.; Pople, J.A. The effect of d-functions on molecular orbital energies for hydrocarbons. *Chem. Phys. Lett.* **1972**, 16, 217-219.

22. Zhurko, G.A.; Zhurko, D.A. Chemcraft - graphical program for visualization of quantum chemistry computations. *Academic version 1.5*, Ivanovo: Russia; **2004**.
23. Philips-Invernizzi, B.; Dupont, D.; Caze, C. Bibliographical review for reflectance of diffusing media. *Opt. Eng.* **2001**, 40, 082-1092.
24. Mishra, V.; Warshi, M.K.; Sati, A.; Kumar, A.; Mishra, V.; Sagdeo, A.; Kuma, R.; Sagdeo, P.R. Diffuse reflectance spectroscopy: An effective tool to probe the defect states in wide band gap semiconducting materials. *Mater. Sci. Semicond. Process.* **2018**, 86, 151-156.
25. Altalhi, T.; Gobouri, A.A.; Refat, M.S.; El-Nahass, M.M.; Hassanien, A.M.; Atta, A.A.; Saad, H.A.; Alhazaa, A.N. Structural, electrochemical and optical properties of 1,2,4-triazine derivative. *Appl. Phys. A* **2020**, 126, 815.
26. Landi Jr., S.; Segundo, I.R.; Freitas, E.; Vasilevskiy, M.; Carneiro, J.; Tavares, C.J. Use and misuse of the Kubelka-Munk function to obtain the band gap energy from diffuse reflectance measurements. *Solid State Commun.* **2022**, 341, 114573.
27. Landi Jr, S. Comment on Photocatalytic degradation of RhB from an aqueous solution using Ag_3PO_4/N-TiO_2 heterostructure and Evaluation of the effect of dose change of Fe_3O_4 nanoparticles on electrochemical biosensor compatibility using hydrogels as an experimental living organism model. *J. Mol. Liq.* **2021**, 338, 116635.
28. Yuan, R.; Guo, M.; Li, C.; Chen, S.; Liu, G.; He, J.; Wan, G.; Fan, N. Detection of early bruises in jujubes based on reflectance, absorbance and Kubelka-Munk spectral data. *Postharvest Biol. Technol.* **2022**, 185, 111810.
29. Jamil, H.; Dildar, I.M.; Ilyas, U.; Hashmi, J.Z.; Shaukat, S.; Sarwar, M.N.; Khaleeq-ur-Rahman, M. Microstructural and optical study of polycrystalline manganese oxide films using Kubelka-Munk function. *Thin Solid Films* **2021**, 732, 138796.
30. Kumar, G.A.; Thomas, J.; George, N.; Kumar, B.A.; Shnan, P.R.; Poori, V.P.N.; Vallabhan, C.P.G.; Unnikrishnan, N.V. Optical absorption studies of free (H_2Pc) and rare earth (RePc) phthalocyanine doped borate glasses. *Phys. Chem. Glass B* **2000**, 41, 89-93.
31. Gouterman, M. Study of the effects of substitution on the absorption spectra of porphin. *J. Chem. Phys.* **1959**, 30, 1139-1161.

32. El-Nahass, M.M.; Hassanien, A.M.; Khusayfan, N.M. Optical characterizations of thermally evaporated perylene-66 (dye content 40%) thin films. *Solid State Commun.* **2013**, 154, 51-55.
33. El-Nahass, M.M.; El-Deeb, A.F.; Metwally, H.S.; El-Sayed, H.E.A.; Hassanien, A.M. Influence of X-ray irradiation on the optical properties of iron(III) chloride tetraphenylporphyrin thin films. *Solid State Sci.* **2010**, 12, 552-557.
34. Mott, N.F.; Davis, E.A. *Electronic Process in the Non-Crystalline Materials*, 2ed ed., Clarendon Press/Oxford University: New York; **1979**.
35. Algradee, M.A.; Elbashar, Y.H.; Alwany, A.B.; Hassan, H.H.; El-Mallawany, R. Impact of Yb_2O_3 on the physical, bonding, dispersion and dielectric properties of Li_2O–ZnO–P_2O_5 glasses. *Mater. Sci. Semicond. Process.* **2022**,140, 106362.
36. Hassanien, A.M.; Altalhi, T.A.; Atta, A.A.; AlHazaa, A.N.; Alsawat, M.; Mersal, G.A.M.; Adam, A.A.; Refat, M.S. Studying spectroscopic, cyclic voltammetry, electrical properties of novel 4-amino antipyrine derivative for photonic applications. *J. Mol. Struc.* **2023**, 1272 134201.
37. Fox, M. *Optical Properties of Solids*, Oxford University Press Inc.: New York; **2001**.
38. Costa, J.C.S.; Taveira, R.J.S.; Lima, C.F.R.A.C.; Mendes, A.; Santos, L.M.N.B.F. Optical band gaps of organic semiconductor materials. *Opt. Mater.* **2016**, 58, 51-60.
39. Bhadwal, A.S.; Tripathi, R.M.; Gupta, R.K.; Kumar, N.; Singh, R.P.; Shrivastav, A. Biogenic synthesis and photocatalytic activity of CdS nanoparticles. *RSC Adv.* **2014**, 4, 9484-9490.
40. Souri, D.; Tahan, Z.E. A new method for the determination of optical band gap and the nature of optical transitions in semiconductors. *Appl. Phys. B* **2015**, 119, 273-279.

41. Rammah, Y.S.; El-Agawany, F.I.; Mahmoud, K.A; El-Mallawany, R.; Ilik, E.; Kilic, G. FTIR, UV–Vis–NIR spectroscopy, and gamma rays shielding competence of novel ZnO-doped vanadium borophosphate glasses. *J. Mater. Sci.: Mater. Electron.* **2020**, 31, 9099-9113.
42. Hassanien, A.M. Surface topology, optical spectroscopic and electrical studies on boron subphthalocyanine chloride thin films. *J. Dispers. Sci. Technol.* **2021** DOI: 10.1080/01932691.2021.1924189.
43 Cheng, H.; Wu, Y.; Su, J.; Wang, Z.; Ghimire, R.P.; Liang, M.; Sun, Z.; Xue, S. Organic dyes containing indolodithienopyrrole unit for dye-sensitized solar cells. *Dyes Pigm.* **2018**, 149 16-24.
44. Kong, Z.; Liu, D.; He, J.; Wang, X. Electrode buffer layers producing high performance nonvolatile organic write-once-read-many-times memory devices. *RSC Adv.* **2017**, 7, 13171-13176.
45. One dimensional ternary Cu–Bi–S based semiconductor nanowires: synthesis, optical and electrical properties. *J. Mater. Chem.* **2012**, 22, 17813-17819.
46. Khan, M.D.; Shakya, S.; Vu, H.H.T.; Habte, L.; Ahn, J.W. Low concentrated phosphorus sorption in aqueous medium on aragonite synthesized by carbonation of seashells: Optimization, kinetics, and mechanism study. *J. Environ. Manage.* **2021**, 280, 111652.
47. Murugavel, S.; Ravikumar, C.; Jaabil, G.; Alagusundaram, P. Synthesis, crystal structure analysis, spectral investigations (NMR, FT-IR, UV), DFT calculations, ADMET studies, molecular docking and anticancer activity of 2-(1-benzyl-5-methyl-1H-1, 2, 3-triazol-4-yl)-4-(2-chlorophenyl)-6-methoxypyridine–a novel potent human topoisomerase IIα inhibitor. *J. Mol. Struct.* **2019**, 1176, 729-742.
48. Al-Hazmi, G.H.; Hassanien, A.M.; Atta, A.A.; Refat, M.S.; Saad, H.A.; Shakya, S.; Adam, A.M.A. Supramolecular charge-transfer complex generated by the interaction between tin(II) 2,3-naphtalocyanine as a donor with DDQ as an acceptor: Spectroscopic studies in solution state and theoretical calculations. *J. Mol. Liq.* **2022**, 362, 119757.
49. Hassanien, A.M.; Altalhi, T.A.; Refat, M.S.; Shakya, S.; Atta, A.A.; Alsawat, M.; Al-Hazaa, A.N.; Asla, K.A. Exploring microstructural, optical, electrical, and DFT/TD-DFT studies of boron subphthalocyanine chloride for renewable energy applications. *Optik* **2022**, 263, 169367.
50. Alkathiri, A.A.; Atta, A.A.; Refat, M.S.; Shakya, S.; Hassanien, A.M.; Algarni, S.A.; Ahmed, E.M.A.; Alomariy, S.E.; Alsawat, M.; Algethami, N. Impedance spectroscopy and DFT/TD-DFT studies of diyttrium trioxide for optoelectronic fields. *J. Rare Earths* **2022**, https://doi.org/10.1016/j.jre.2022.03.010.